

Origin of layer dependence in band structures of two-dimensional materials

Mit H. Naik and Manish Jain

Center for Condensed Matter Theory, Department of Physics, Indian Institute of Science, Bangalore 560012, India

(Received 17 October 2016; revised manuscript received 1 March 2017; published 18 April 2017)

We study the origin of layer dependence in band structures of two-dimensional (2D) materials. We find that the layer dependence, at the density functional theory (DFT) level, is a result of quantum confinement and the nonlinearity of the exchange-correlation functional. We use this to develop an efficient scheme for performing DFT and GW calculations of multilayer systems. We show that the DFT and quasiparticle band structures of a multilayer system can be derived from a single calculation on a monolayer of the material. We test this scheme on multilayers of MoS_2 , graphene, and phosphorene. This new scheme yields results in excellent agreement with the standard methods at a fraction of the computation cost. This helps overcome the challenge of performing fully converged GW calculations on multilayers of 2D materials, particularly in the case of transition-metal dichalcogenides, which involve very stringent convergence parameters.

DOI: [10.1103/PhysRevB.95.165125](https://doi.org/10.1103/PhysRevB.95.165125)

I. INTRODUCTION

Two-dimensional (2D) materials have been extensively studied in the last decade [1–9] owing to their applications in electronics and optoelectronics [10–12]. 2D materials consist of layers that are held together by weak van der Waals forces. A remarkable feature of these layered materials is the difference in properties of a monolayer compared to multilayers of the same material [2–7,13,14]. For instance, monolayer of MoS_2 has a direct band gap, while multilayers of MoS_2 have an indirect gap [2,3,5,13,15]. Most gapped 2D materials, such as transition-metal dichalcogenides (TMDCs), hexagonal boron nitride, and phosphorene, show an unmistakable reduction in band gap with the number of layers [2,3,6,7,13–20].

First-principles electronic structure calculations, based on the GW [21,22] approximation, have resulted in band gaps that are in excellent agreement with experiments [6,8,16,23–27] on these materials. Band gaps of these materials calculated using density functional theory (DFT) [28,29], while underestimated, also show a clear reduction with the number of layers [7,14,15,18–20]. Most studies have attributed this reduction in the band gap to quantum confinement [3,5–7]. However, there are no studies that quantitatively explain this trend.

The idea of quantum confinement comes from the model of an electron in a one-dimensional box. In multilayer stacks of 2D materials, the confining length of the box is directly proportional to the number of layers. In this context, the increase in the confinement length in multilayers as compared to a monolayer, due to the summing of constituent layer potentials, is attributed to quantum confinement. On adding the potentials of constituent layers, the interlayer spacing creates a finite barrier in the interstitial region between adjacent layers. This barrier with a DFT-calculated Hartree potential profile has been used to qualitatively explain the trend in the layer dependence of the band gap in phosphorene [6]. Recently, perturbation approaches [18,30], which need input from explicit multilayer calculations, have been used to study layer dependence of band structures.

Furthermore, in the case of TMDCs, it has been shown that the quasiparticle band gap calculated using the GW approximation converges extremely slowly with the number of unoccupied states, k -point sampling, and the screened

Coulomb cutoff [31,32]. Performing separate GW calculations for a monolayer, bilayer, trilayer, or more with parameters that ensure convergence is computationally very challenging. To study the variation of properties as a function of interlayer spacing or stacking of the layers needs one to repeat the calculation for different parameters. Moreover, GW calculations on heterostructures of 2D materials are presently intractable due to their lattice incommensurability necessitating the use of large supercells of each material. Identifying the origin of layer dependence opens up the possibility of deriving ground-state and excited-state properties of multilayer stacks from calculations on a monolayer alone. Doing so would immensely ease the computation cost incurred in performing separate DFT and GW calculations for different configurations of the constituent layers.

We study the physical origin of layer dependence in band structures of 2D materials. We show that while quantum confinement gives qualitatively the right trend, the nonlinearity of the V_{xc} functional plays a crucial role in quantitatively determining the layer dependence. We show that within DFT, band structures of multilayer stacks can be derived from a single calculation on a monolayer of the material. We also extend this scheme to obtain quasiparticle energies of multilayer systems from a single GW calculation on a monolayer of the material. We apply this method to understand the layer dependence of band structure in multilayers of a prototypical TMDC, 2H- MoS_2 , and compare the results to the standard calculations on this material [2–4]. We demonstrate the transferability of this scheme by applying it to graphene and phosphorene.

II. COMPUTATION DETAILS

We performed the DFT calculations using the plane-wave pseudopotential method as implemented in the QUANTUM ESPRESSO [33] package. Norm-conserving pseudopotentials were used in all calculations. The wave functions were expanded in plane waves with an energy cutoff of 150 Ry for MoS_2 . For graphene and phosphorene, we used a wave function cutoff of 70 Ry and 40 Ry, respectively. The local density approximation to the exchange-correlation functional

[34] was used in MoS₂ and graphene calculations. For phosphorene we used the Perdew-Burke-Ernzerhof exchange-correlation functional [35]. The Brillouin zone was sampled with $24 \times 24 \times 1$, $21 \times 21 \times 1$ and $21 \times 15 \times 1$ k -point grids for MoS₂, graphene, and phosphorene, respectively. We kept the in-plane lattice parameter for each material fixed in all the calculations. The bilayer and trilayer were constructed from the monolayer with the appropriate stacking and interlayer spacing. No atomic relaxations were allowed in the bilayer and trilayer. The supercell dimension in the out-of-plane direction was fixed at 35 Å.

The GW calculations were performed using the BERKELEYGW package [36,37]. For MoS₂, the dielectric function was evaluated with plane waves up to a cutoff of 35 Ry and was extended to finite frequencies using the generalized plasmon pole (GPP) [22] model. The self-energy was constructed using the one-shot G_0W_0 method. The Coulomb interaction was truncated in the out-of-plane direction [38]. For MoS₂ supercell size of 35 Å in the out-of-plane direction, $24 \times 24 \times 1$ k -point sampling and 8400 valence and conduction states are necessary to ensure convergence [32]. We perform separate calculations on monolayer, bilayer, and trilayer MoS₂ with $12 \times 12 \times 1$ k -point sampling and 6000 valence and conduction states and compare the quasiparticle band structures of bilayer and trilayer with results obtained from the proposed scheme. These parameters, while not fully converged, demonstrate the efficacy of this scheme. We also perform fully converged calculations on a monolayer of MoS₂ and derive the band gap, ionization potential, and electron affinity of bilayer and trilayer using our scheme. Our fully converged monolayer band gap is in good agreement with previous calculations [8,32]. For phosphorene, we perform separate calculations on monolayer, bilayer, and trilayer with $21 \times 15 \times 1$ k -point sampling, 800 valence and conduction states, and 15 Ry dielectric cutoff. We compare the band gap, ionization potential, and electron affinity obtained using our scheme to those obtained from the full calculation. The static remainder technique was used to speed up convergence with the number of bands [39] in all calculations.

III. DFT BAND STRUCTURES

In order to understand the layer dependence of the DFT band gap, consider a bilayer of MoS₂ with constituent layers labeled “a” and “b” [Fig. 1(a)] [40]. We perform separate DFT calculations on layer a, layer b, and the bilayer to obtain the self-consistent charge densities and potentials of each. In Fig. 1(b), we plot the planar averaged charge densities of layer a, layer b, and the bilayer. From the figure one can see that the bilayer charge density, ρ^{bi} , lies on top of the sum of the charge densities of the constituent layers, $\rho^a + \rho^b$, which indicates that there is no significant rearrangement of charge in the bilayer compared to the monolayers. Figure 1(c) shows the planar averaged total DFT potential of the bilayer, $V_{\text{tot}}^{\text{bi}}$. From this figure, it is clear that the sum of the layer potentials $V_{\text{tot}}^a + V_{\text{tot}}^b$ is not equal to the bilayer potential. The sum of the potentials, as described above, is the use of quantum confinement to obtain the potential for the bilayer. The difference, $V_{\text{tot}}^{\text{bi}} - (V_{\text{tot}}^a + V_{\text{tot}}^b)$, is localized to the interstitial region between the two layers where the charge densities

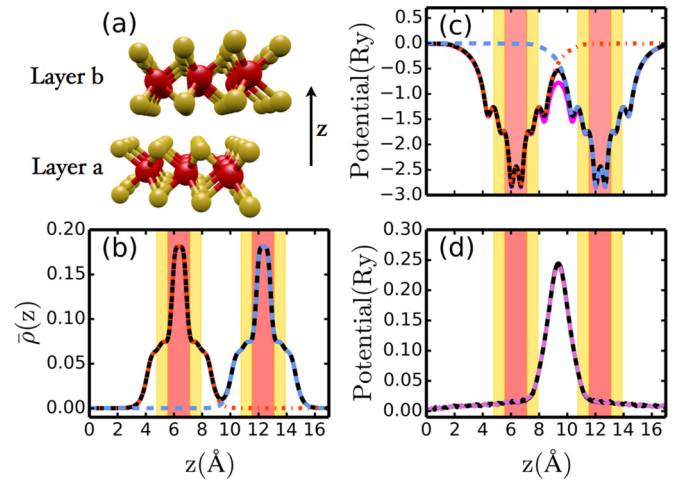


FIG. 1. (a) Bilayer MoS₂ in AB stacking, red spheres represent Mo atoms and yellow spheres S atoms. (b) Planar averaged charge density of bilayer MoS₂ (black solid line), planar averaged charge density of layer “a” (red dash-dot line), layer “b” (blue dashed line) and sum of layer a and b (magenta line not seen). The shaded regions indicate the position of the MoS₂ layers in the simulation cell. (c) Planar averaged DFT potential of the layer a, V_{tot}^a (red dash-dot line), layer b, V_{tot}^b (blue dashed line), the sum $V_{\text{tot}}^a + V_{\text{tot}}^b$ (solid magenta line), and bilayer, $V_{\text{tot}}^{\text{bi}}$ (black solid line). (d) Difference $V_{\text{tot}}^{\text{bi}} - (V_{\text{tot}}^a + V_{\text{tot}}^b)$ (black solid line) and $V_{xc}[\rho^a + \rho^b] - (V_{xc}[\rho^a] + V_{xc}[\rho^b])$ (violet dashed line).

overlap. It can not arise from the Hartree potential since it is a linear functional of the charge density and here the charge density of the bilayer is a sum of the charge densities of the individual layers. It can not arise from the ionic potential either, due to the absence of atomic relaxations in the bilayer. The difference must arise due to the nonlinearity of the exchange-correlation functional. Figure 1(d) plots this difference, which is an additional barrier between the layers. Figure 1(d) also plots $V_{xc}[\rho^a + \rho^b] - (V_{xc}[\rho^a] + V_{xc}[\rho^b]) = \Delta V_{xc}$, showing that this additional barrier indeed comes solely from the exchange-correlation difference. The total bilayer potential can thus be expressed as a sum of the individual layer potentials and ΔV_{xc} . Thus, the layer dependence of properties is an effect of quantum confinement and nonlinearity of the V_{xc} functional.

We can construct the DFT Hamiltonian for the bilayer in terms of the potential and charge density of the constituent layers as:

$$H = \hat{T} + V_{\text{tot}}^a + V_{\text{tot}}^b + \Delta V_{xc}, \quad (1)$$

where \hat{T} is the kinetic energy operator. It should be noted that everything required to construct this Hamiltonian can be obtained from a single monolayer calculation, say on layer a. Based on the relative configuration of atoms in layer b with respect to layer a, a suitable transformation can be applied on ρ^a and V_{tot}^a to obtain ρ^b and V_{tot}^b , respectively. The wave functions of layer a, $\{\psi_{nk}^a\}$, can similarly be transformed to obtain the wave functions of layer b, $\{\psi_{nk}^b\}$. The Hamiltonian can then be constructed in the basis of the wave functions of the two layers, $\{\psi^a, \psi^b\}$, keeping in mind that the wave functions of the two layers do not form an orthogonal basis. The generalized eigenvalue problem can be solved to yield eigenvalues

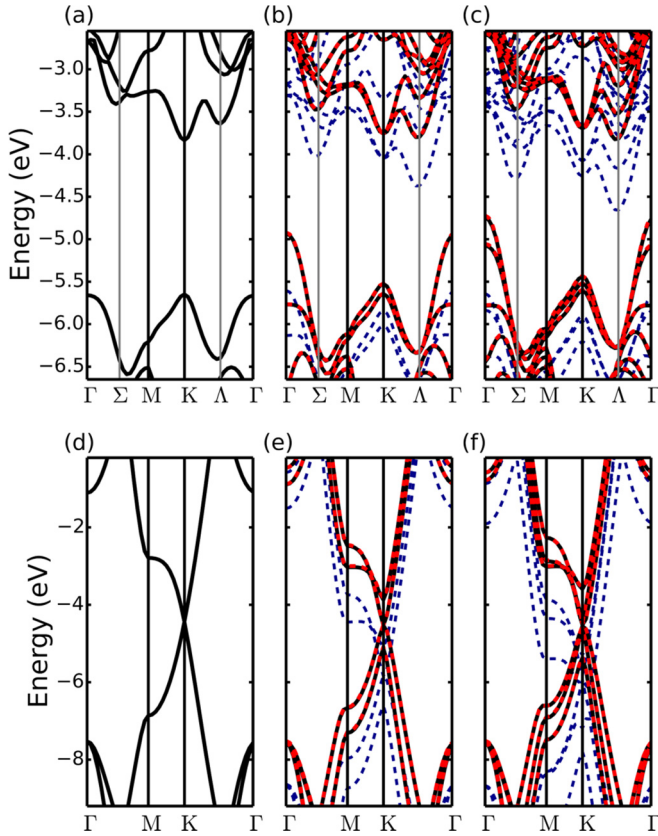


FIG. 2. (a), (b), and (c) plot the DFT band structure of monolayer, bilayer, and trilayer MoS₂, respectively. (d), (e), and (f) plot the DFT band structures of monolayer, bilayer, and trilayer graphene. The black solid line indicates the result from separate DFT calculations on these systems. The red dashed line shows the result obtained by a single-shot diagonalization of the constructed Hamiltonian Eq. (1) for these systems in the basis of the wave functions of the constituent layers. The blue dashed lines are the eigenvalues obtained by considering only quantum confinement in these systems.

and eigenfunctions of the bilayer. This procedure can easily be generalized to N layers: $H = \hat{T} + \sum_{i=1}^N V_{\text{tot}}^i + \Delta V_{xc}$; where $\Delta V_{xc} = V_{xc}[\sum_{i=1}^N \rho^i] - \sum_{i=1}^N V_{xc}[\rho^i]$. It is worth noting that while constructing the Hamiltonian we use $V_{xc}(\mathbf{r})$ and not just the planar averaged quantities.

The band structure of monolayer, bilayer, and trilayer MoS₂ from separate DFT calculations is plotted in Figs. 2(a), 2(b), and 2(c), respectively. The points Σ and Λ are marked halfway between Γ -M and K- Γ respectively. Figures 2(d), 2(e), and 2(f) similarly show the band structure of monolayer, bilayer, and trilayer graphene, respectively. Figure 2 also shows the band structure obtained by neglecting ΔV_{xc} from Eq. (1). This describes the effect of quantum confinement alone on the layer dependence of the band structures. While it captures the qualitative trends such as the transition from direct to indirect band gap in MoS₂, it fails to give an accurate layer dependence of the value of the band gap, ionization potentials, and level splittings in the band structure. In MoS₂, the splittings are overestimated at the conduction band minimum (CBM) of the Λ point and underestimated at the Γ point valence band maximum (VBM). The relative

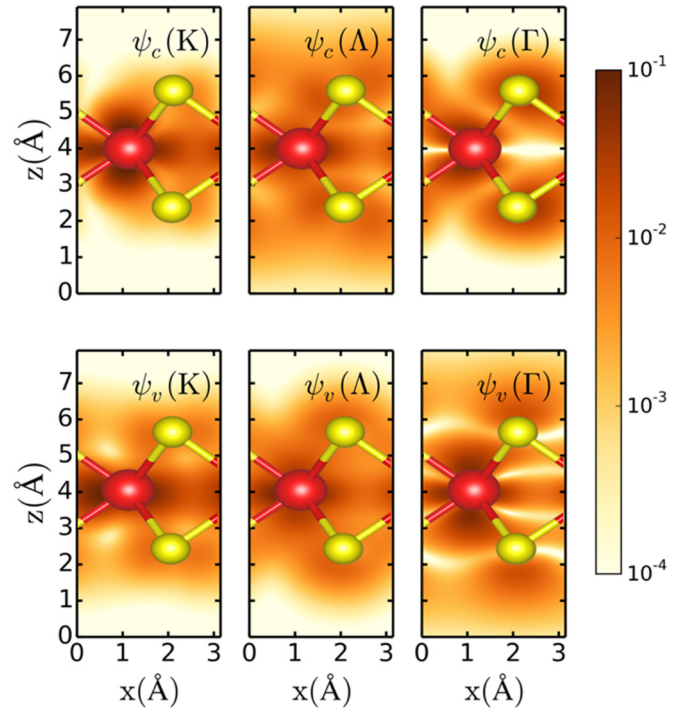


FIG. 3. Modulus squared wave functions of monolayer MoS₂, integrated out along [010] lattice vector direction. z is the out-of-plane direction and x the [100] direction. Top: CBM wave functions at K, Λ , and Γ points, respectively. Bottom: VBM wave functions at K, Λ , and Γ points, respectively.

positions of the conduction band edges at the Λ , K, and Σ points are also very different from the full DFT calculation. Similarly, in graphene, excluding ΔV_{xc} overestimates the ionization potential and the band splittings. The band structure obtained from the eigenvalues obtained by diagonalizing the constructed Hamiltonian described previously is also plotted in Fig. 2. As can be seen, these band structures are in excellent agreement with the full calculation for MoS₂ and graphene. A slight difference up to 5–10 meV is found due to a small rearrangement of charge in the bilayer or trilayer as compared to the sum of the constituent layer charge densities. Hence, to obtain the quantitative layer dependence, both the effects of quantum confinement and nonlinearity of the exchange-correlation functional need to be accounted for.

The band structures of MoS₂ in Fig. 2 show a transition from a direct band gap at K in the monolayer to an indirect band gap from Γ to Λ in the bilayer. The transition is driven by the large splitting of the VBM at the Γ point and CBM at the Λ point. The K point VBM and CBM on the other hand split only slightly. The amount by which a band splits depends on the off-diagonal elements of the multilayer Hamiltonian represented in the basis of the constituent layer wave functions and the overlap between the wave functions of the constituent layers. The VBM and CBM of the monolayer at K are localized in space and have a large Mo d orbital character (see Fig. 3). The CBM at Λ and VBM at Γ on the other hand have a strong S p_z character (see Fig. 3). They are hence more delocalized in the out-of-plane direction and hybridize more with the wave functions of other layers than the wave functions at K. This

leads to the large splittings in the band structure at these points for the bilayer and trilayer [see Figs. 2(b) and 2(c)]. The VBM and CBM at K, VBM at Λ , and CBM at Γ show little to no splitting in the band structures owing to their localized nature (see Fig. 3).

IV. QUASIPARTICLE BAND STRUCTURES

We can extend this method to calculate the quasiparticle energies and band structures. The DFT eigenvalues can be corrected by using the GW approximation to the electron self-energy, Σ [22]. For the bilayer, quasiparticle eigenvalues are given by:

$$\epsilon_i^{\text{QP}} = \epsilon_i^{\text{DFT}} + \langle \psi_i^{\text{bi}} | \Sigma^{\text{bi}}(\epsilon_i^{\text{QP}}) - V_{xc}^{\text{bi}} | \psi_i^{\text{bi}} \rangle,$$

where $|\psi_i^{\text{bi}}\rangle$ is the DFT wave function corresponding to the eigenvalue ϵ_i^{DFT} and ϵ_i^{QP} is the corresponding quasiparticle energy. Evaluating Σ^{bi} with the one-shot G_0W_0 method within the GPP approximation [22] requires the bilayer charge density, the bilayer irreducible polarizability, χ_0^{bi} , and wave functions of the bilayer, ψ^{bi} .

We now show that all the required quantities can be approximated from the quantities obtained from a monolayer calculation, say on layer a. The procedure to obtain ψ^{bi} and ρ^{bi} is as described before. The bilayer self-energy can be written as a sum over the individual self-energies of the layers and a correction term:

$$\langle \psi^{\text{bi}} | \Sigma^{\text{bi}} | \psi^{\text{bi}} \rangle = \langle \psi^{\text{bi}} | \Sigma_{GW}^a + \Sigma_{GW}^b | \psi^{\text{bi}} \rangle + \langle \psi^{\text{bi}} | \Delta \Sigma | \psi^{\text{bi}} \rangle. \quad (2)$$

$\langle \psi^{\text{bi}} | \Sigma_{GW}^a | \psi^{\text{bi}} \rangle$ can be computed directly from monolayer irreducible polarizability, χ_0^a , ρ^a , and ψ^a . To compute $\langle \psi^{\text{bi}} | \Sigma_{GW}^b | \psi^{\text{bi}} \rangle$, we obtain χ_0^b , ρ^b , and ψ^b by applying transformations similar to the ones described above to χ_0^a , ρ^a , and ψ^a respectively. The correction term, $\langle \psi^{\text{bi}} | \Delta \Sigma | \psi^{\text{bi}} \rangle$ contains information on the interaction between the layers. Due to the weak coupling between the layers, we expect $\langle \psi^{\text{bi}} | \Delta \Sigma | \psi^{\text{bi}} \rangle$ to be a small correction (compared to $\langle \psi^{\text{bi}} | \Sigma^a + \Sigma^b | \psi^{\text{bi}} \rangle$). We can evaluate $\Delta \Sigma$ at various levels of approximation. It can be evaluated at the DFT level by $\Delta \Sigma = \Delta V_{xc}$; or assuming just exchange interaction between the layers $\Delta \Sigma_x = \Sigma_x^{\text{bi}} - \Sigma_x^a - \Sigma_x^b$; or within the static limit of GW (COHSEX) $\Delta \Sigma_{\text{COHSEX}} = \Sigma_{\text{COHSEX}}^{\text{bi}} - \Sigma_{\text{COHSEX}}^a - \Sigma_{\text{COHSEX}}^b$; or within full GW . The only additional quantity needed in some of these approximations is, χ_0^{bi} , which can be approximated as a sum of the irreducible polarizability of constituent layers: $\chi_0^{\text{bi}} = \chi_0^a + \chi_0^b$ [24,25]. This method can easily be extended to calculate band structures of n layers by computing $\langle \psi^n | \Sigma^n | \psi^n \rangle = \langle \psi^n | \sum_{i=1}^n \Sigma_{GW}^i | \psi^n \rangle + \langle \psi^n | \Delta \Sigma | \psi^n \rangle$. $\Delta \Sigma = \Sigma^n - \sum_{i=1}^n \Sigma^i$ can then be evaluated at an appropriate level of approximation.

Table I shows the ionization potential, electron affinity, and band gap for bilayer and trilayer MoS₂ for different approximations to $\Delta \Sigma$. We compare them to the full GW calculation on these systems. $\Delta \Sigma = \Delta V_{xc}$ and $\Delta \Sigma = \Delta \Sigma_{\text{COHSEX}}$ show good agreement with the converged gap for the bilayer but fail to give the right ionization potential (IP) and electron affinity (EA). The COHSEX approximation to $\Delta \Sigma$ works well for the band gap in trilayer too, but again falls short in the ionization

TABLE I. Ionization potential (IP), electron affinity (EA), and band gap (in eV) of bilayer and trilayer MoS₂ evaluated using the constructed Σ for various approximations of $\Delta \Sigma$ described in the text. The top section compares the results from full calculations performed with $12 \times 12 \times 1$ sampling, 6000 bands to the results from various approximations of $\Delta \Sigma$. $\Delta \Sigma_{GW}^{800}$ denotes $\Delta \Sigma$ evaluated at the GPP level with 800 bands. The bottom section are the results obtained by applying our scheme to a fully converged monolayer calculation.

$\Delta \Sigma$	Bilayer			Trilayer		
	IP	EA	Gap	IP	EA	Gap
($12 \times 12 \times 1$)						
ΔV_{xc}	5.49	3.38	2.11	4.84	2.75	2.09
$\Delta \Sigma_x$	7.09	4.26	2.83	7.04	4.56	2.49
$\Delta \Sigma_{\text{COHSEX}}$	5.65	3.55	2.10	4.98	3.33	1.65
$\Delta \Sigma_{GW}^{800}$	6.16	3.99	2.17	5.86	4.11	1.75
Full	6.17	4.03	2.14	5.87	4.17	1.70
$\Delta \Sigma$	Bilayer			Trilayer		
($24 \times 24 \times 1$)	IP	EA	Gap	IP	EA	Gap
$\Delta \Sigma_{GW}^{800}$	6.05	4.03	2.02	5.81	4.09	1.72

potential and electron affinity. The difference in band gap obtained using $\Delta \Sigma = \Delta \Sigma_{\text{COHSEX}}$ and $\Delta \Sigma = \Delta \Sigma_x$ shows that correlation plays an important role in the interaction between the layers. As the next level of approximation, we compute $\Delta \Sigma$ using GW with a few number, N_c , of conduction states. We find that a small number, $N_c = 800$, is sufficient to converge the bilayer and trilayer MoS₂ self-energies. Figures 4(a) and 4(b) show this convergence. It should be noted that the small number of states are used here only to compute the $\Delta \Sigma$. We do not calculate χ_0^{bi} with a few unoccupied states. The bilayer irreducible polarizability is constructed with

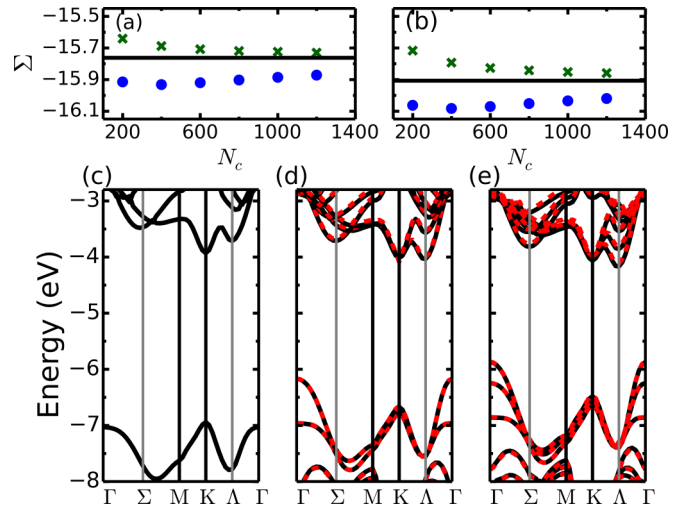


FIG. 4. (a) and (b) Convergence of the constructed $\langle \psi_{CBM} | \Sigma^{\text{bi}} | \psi_{CBM} \rangle$ and $\langle \psi_{CBM} | \Sigma^{\text{tri}} | \psi_{CBM} \rangle$ with the number of bands for the CBM at Λ (green crosses). The horizontal line is the converged result from full calculations. The blue circles show the slow convergence of the full calculation with the usual procedure. (c), (d), and (e) plot the quasiparticle band structure of monolayer, bilayer and trilayer MoS₂, respectively. The black solid line indicates the result from separate GW calculations. The red dashed line shows the result obtained using the scheme described in the text.

TABLE II. Ionization potential (IP), electron affinity (EA), and band gap (in eV) of bilayer and trilayer phosphorene evaluated using the constructed Σ for various approximations of $\Delta\Sigma$ described in the text. $\Delta\Sigma_{GW}^{300}$ denotes $\Delta\Sigma$ evaluated at the GPP level with 300 bands.

$\Delta\Sigma$	Bilayer			Trilayer		
	IP	EA	Gap	IP	EA	Gap
ΔV_{xc}	5.47	3.71	1.76	5.12	3.74	1.38
$\Delta\Sigma_x$	6.45	4.62	1.83	6.66	4.86	1.80
$\Delta\Sigma_{\text{COHSEX}}$	5.27	3.69	1.58	4.69	3.60	1.09
$\Delta\Sigma_{GW}^{300}$	5.73	4.17	1.56	5.50	4.25	1.25
Full	5.73	4.20	1.53	5.49	4.29	1.20

the converged monolayer irreducible polarizabilities. With this approximation, we obtain the IP, EA, and band gap in good agreement with the full calculation [see Table I]. A major computational bottleneck in performing separate GW calculations for the monolayer, bilayer, and trilayer is the generation of the large number of unoccupied bands on a fine k -point grid and using these to compute the irreducible polarizability. This scheme completely does away with the need to regenerate the unoccupied bands and the polarizability for the bilayer and trilayer once we have the same for a monolayer. Figures 4(d) and 4(e) compare the bilayer and trilayer MoS_2 quasiparticle band structures obtained using this scheme with those obtained from full calculations on these. The eigenvalues are in good agreement with the full GW calculation, up to 100 meV, and obtained at a small fraction of the computation cost. Note that the results in Fig. 4 and Table I were obtained with slightly softened convergence parameters (see Sec. II). We also perform a monolayer calculation with the fully converged parameters and use this scheme to derive the band gap, IP, and EA for bilayer and trilayer [see Table I]. The converged IP, EA, and band gap for the monolayer are found to be 6.76, 4.02, and 2.74 eV, respectively. The band gap for the monolayer is found to be in good agreement with previous calculations [8,32].

Table II compares the IP, EA, and band gap for bilayer and trilayer phosphorene obtained using this scheme to those obtained from the full calculation on these. Here we find that $N_c = 300$ is sufficient to converge the bilayer and trilayer self-energies. The COHSEX approximation to $\Delta\Sigma$ again shows good agreement with the full calculation for the band gap (up to 100 meV), but fails to give the right IP and EA. Evaluating $\Delta\Sigma$ at the COHSEX level thus seems to be a consistent approximation to obtain the converged quasiparticle band gap.

V. INTERLAYER SPACING DEPENDENCE IN BILAYER

The transition in bilayer MoS_2 , from interacting monolayers to noninteracting ones can be studied by gradually increasing the interlayer spacing. Figure 5 shows the evolution of the DFT band structure, charge density, and potential of bilayer MoS_2 as a function of increasing interlayer spacing d . The equilibrium spacing is $d_{\text{eq}} = 6 \text{ \AA}$. As the spacing between the layers increase, the interaction between them weakens and the splitting of the valence bands at Γ and

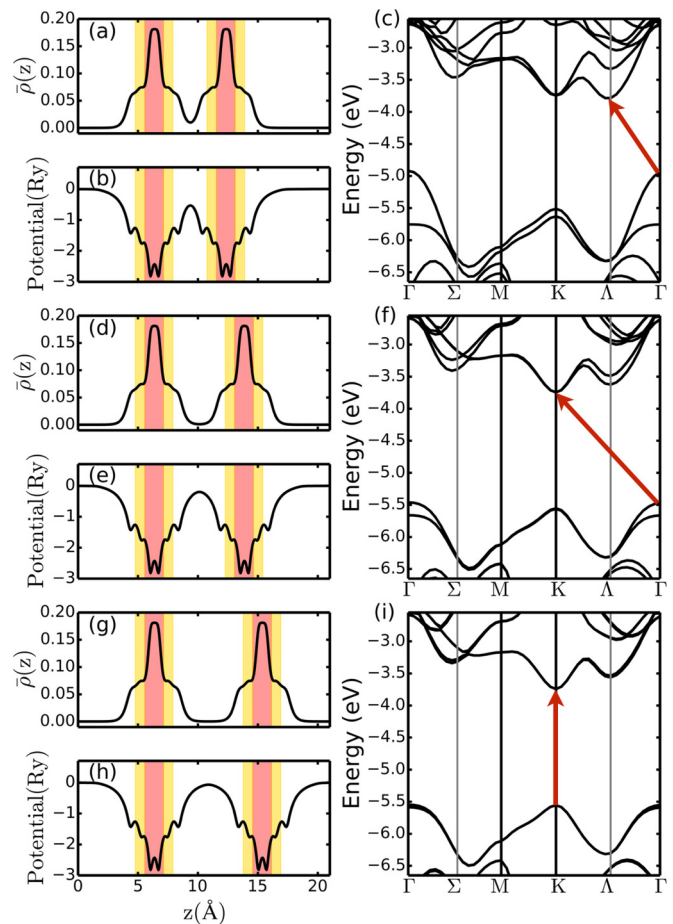


FIG. 5. (a), (b), and (c) DFT charge density, potential, and band structure of bilayer MoS_2 at the equilibrium interlayer spacing of 6.0 \AA , respectively. (d), (e), and (f) For interlayer spacing of 7.5 \AA . (g), (h), and (i) For interlayer spacing of 9.0 \AA .

the conduction bands at Λ reduces. This leads to a band-gap transition from Γ - Λ to Γ - K to K - K . At $d = 7.5 \text{ \AA}$, the charge densities of the two layers stop overlapping, but the potential barrier between the layers is not zero. At this point the layers are weakly interacting and the nature of interaction within DFT is purely due to quantum confinement; ΔV_{xc} is zero. At $d = 9 \text{ \AA}$ and above, the two layers are completely noninteracting at the DFT level and the gap is that of monolayer MoS_2 .

We construct the bilayer self energy at different interlayer spacings using the various approximations to $\Delta\Sigma$. The gap thus computed is shown in Fig. 6(a). In the approximation of $\Delta\Sigma = \Delta\Sigma_x$ and $\Delta\Sigma = \Delta V_{xc}$, the layers become noninteracting once the charge densities of the two layers stop overlapping. Thus, the gap in this approximation goes to the monolayer gap for spacing larger than $d = 7.5 \text{ \AA}$. The approximations of $\Delta\Sigma = \Delta\Sigma_{\text{COHSEX}}$ and $\Delta\Sigma = \Delta\Sigma_{GW}^{800}$ include the long-range correlation interaction between the layers. The band gap computed in these approximations thus show a slower convergence to the monolayer gap with increasing interlayer spacing. Note that these calculations are performed using a coarser $12 \times 12 \times 1k$ -point sampling and 6000 bands, leading to an overestimate of the monolayer gap in

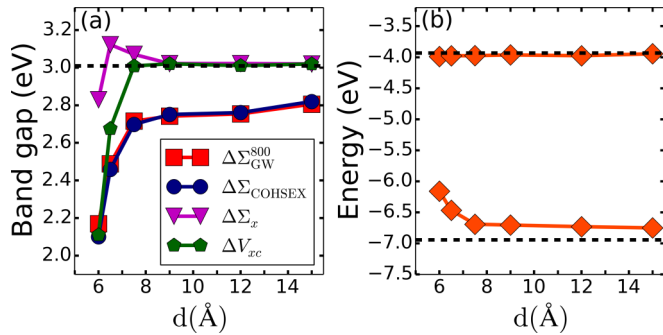


FIG. 6. (a) Band gap of bilayer MoS_2 as a function of interlayer spacing evaluated using the constructed Σ for various approximations to $\Delta\Sigma$. The dashed line marks the monolayer band gap within GW . (b) VBM and CBM of the bilayer as a function of interlayer spacing, evaluated using $\Delta\Sigma = \Delta\Sigma_{GW}^{800}$. The dashed line marks the GW VBM and CBM of a monolayer.

Fig. 6. Figure 6(b) shows the VBM and CBM levels computed using $\Delta\Sigma = \Delta\Sigma_{GW}^{800}$ as a function of increasing interlayer spacing. The bilayer CBM shows a weak dependence on the interlayer spacing and is already aligned with the monolayer CBM, while the bilayer VBM shows a slow convergence towards the monolayer VBM as the spacing is increased. This is similar to the effect of a metallic substrate on a molecule, where DFT shows no renormalization of the band gap but accounting for correlation effects in GW shows a significant renormalization [41–43]. The renormalization of the molecular levels is due to screening from image charge effects, arising from the metal substrate. In the bilayer MoS_2 system, similarly, one monolayer is affected by the screening from the other.

VI. CONCLUSION

We studied the origin of layer dependence in band structures of 2D layered materials and developed a scheme to derive multilayer properties from calculations on a monolayer alone. We showed that the observed trend in layer dependence within DFT is a combined effect of quantum confinement and nonlinearity of the DFT exchange-correlation functional. We also constructed the electron self-energy for multilayers in terms of monolayer irreducible polarizability, charge density, and wave functions. The DFT and quasiparticle band structures obtained using this scheme are in excellent agreement with those from the full calculation. The advantage of this scheme is that it can provide accurate results operating at a small fraction of the computation cost of a full calculation on multilayer systems. We show that using this scheme, one is able to capture the long-range correlation effects within GW , which leads to a significant renormalization of the gap even when DFT finds the layers to be noninteracting at larger interlayer spacings. This scheme can also be useful to study the variation in band structure as a function of stacking between the layers. Furthermore, it can be extended to study the nature of interaction between layers in heterostructures of these materials. It paves a way to derive properties of a heterostructure from just unit cell calculations on the constituent materials. This scheme is a promising tool to study multilayers and layer dependence of properties in the growing family of 2D layered materials.

ACKNOWLEDGMENTS

We thank the Supercomputer Education and Research Centre (SERC) at IISc for providing the computational facilities.

- [1] K. S. Novoselov, D. Jiang, F. Schedin, T. J. Booth, V. V. Khotkevich, S. V. Morozov, and A. K. Geim, *Proc. Nat. Acad. Sci. USA* **102**, 10451 (2005).
- [2] K. F. Mak, C. Lee, J. Hone, J. Shan, and T. F. Heinz, *Phys. Rev. Lett.* **105**, 136805 (2010).
- [3] A. Splendiani, L. Sun, Y. Zhang, T. Li, J. Kim, C.-Y. Chim, G. Galli, and F. Wang, *Nano Lett.* **10**, 1271 (2010).
- [4] Q. H. Wang, K. Kalantar-Zadeh, A. Kis, J. N. Coleman, and M. S. Strano, *Nature Nano* **7**, 699 (2012).
- [5] W. Jin, P.-C. Yeh, N. Zaki, D. Zhang, J. T. Sadowski, A. Al-Mahboob, A. M. van der Zande, D. A. Chenet, J. I. Dadap, I. P. Herman, P. Sutter, J. Hone, and R. M. Osgood, *Phys. Rev. Lett.* **111**, 106801 (2013).
- [6] V. Tran, R. Soklaski, Y. Liang, and L. Yang, *Phys. Rev. B* **89**, 235319 (2014).
- [7] A. Kuc, N. Zibouche, and T. Heine, *Phys. Rev. B* **83**, 245213 (2011).
- [8] D. Y. Qiu, F. H. da Jornada, and S. G. Louie, *Phys. Rev. Lett.* **111**, 216805 (2013).
- [9] H. Liu, A. T. Neal, Z. Zhu, Z. Luo, X. Xu, D. Tománek, and P. D. Ye, *ACS Nano* **8**, 4033 (2014).
- [10] B. Radisavljevic, A. Radenovic, J. Brivio, V. Giacometti, and A. Kis, *Nature Nano* **6**, 147 (2011).
- [11] L. Li, Y. Yu, G. J. Ye, Q. Ge, X. Ou, H. Wu, D. Feng, X. H. Chen, and Y. Zhang, *Nature Nano* **9**, 372 (2014).
- [12] K. Roy, M. Padmanabhan, S. Goswami, T. P. Sai, G. Ramalingam, S. Raghavan, and A. Ghosh, *Nature Nano* **8**, 826 (2013).
- [13] J. K. Ellis, M. J. Lucero, and G. E. Scuseria, *Appl. Phys. Lett.* **99**, 261908 (2011).
- [14] J. Hong, K. Li, C. Jin, X. Zhang, Z. Zhang, and J. Yuan, *Phys. Rev. B* **93**, 075440 (2016).
- [15] J. E. Padilha, H. Peelaers, A. Janotti, and C. G. Van de Walle, *Phys. Rev. B* **90**, 205420 (2014).
- [16] V. Tran, R. Fei, and L. Yang, *2D Materials* **2**, 044014 (2015).
- [17] H.-P. Komsa and A. V. Krasheninnikov, *Phys. Rev. B* **86**, 241201 (2012).
- [18] J. Kang, L. Zhang, and S.-H. Wei, *J. Phys. Chem. Lett.* **7**, 597 (2016).
- [19] X. Fan, D. J. Singh, and W. Zheng, *J. Phys. Chem. Lett.* **7**, 2175 (2016).
- [20] G. Constantinescu, A. Kuc, and T. Heine, *Phys. Rev. Lett.* **111**, 036104 (2013).

- [21] L. Hedin, *Phys. Rev.* **139**, A796 (1965); L. Hedin and S. Lundqvist, in *Advances in Research and Applications*, edited by F. Seitz, D. Turnbull, and H. Ehrenreich, Solid State Physics Vol. 23 (Academic Press, New York, 1970), pp. 1–181.
- [22] M. S. Hybertsen and S. G. Louie, *Phys. Rev. B* **34**, 5390 (1986). *Phys. Rev. Lett.* **55**, 1418 (1985).
- [23] A. J. Bradley, M. M. Ugeda, F. H. da Jornada, D. Y. Qiu, W. Ruan, Y. Zhang, S. Wickenburg, A. Riss, J. Lu, S.-K. Mo, Z. Hussain, Z.-X. Shen, S. G. Louie, and M. F. Crommie, *Nano Lett.* **15**, 2594 (2015).
- [24] M. M. Ugeda, A. J. Bradley, S.-F. Shi, F. H. da Jornada, Y. Zhang, D. Y. Qiu, W. Ruan, S.-K. Mo, Z. Hussain, Z.-X. Shen, F. Wang, S. G. Louie, and M. F. Crommie, *Nature Mater.* **13**, 1091 (2014).
- [25] J. Lischner, D. Vigil-Fowler, and S. G. Louie, *Phys. Rev. Lett.* **110**, 146801 (2013).
- [26] Z. Ye, T. Cao, K. O'Brien, H. Zhu, X. Yin, Y. Wang, S. G. Louie, and X. Zhang, *Nature (London)* **513**, 214 (2014).
- [27] T. Cao, Z. Li, D. Y. Qiu, and S. G. Louie, *Nano Lett.* **16**, 5542 (2016).
- [28] P. Hohenberg and W. Kohn, *Phys. Rev.* **136**, B864 (1964).
- [29] W. Kohn and L. J. Sham, *Phys. Rev.* **140**, A1133 (1965).
- [30] G. A. Tritsarlis, S. N. Shirodkar, E. Kaxiras, P. Cazeaux, M. Luskín, P. Plechá, and E. Cancès, *J. Mater. Res.* **31**, 959 (2016).
- [31] D. Y. Qiu, F. H. da Jornada, and S. G. Louie, *Phys. Rev. Lett.* **115**, 119901(E) (2015).
- [32] D. Y. Qiu, F. H. da Jornada, and S. G. Louie, *Phys. Rev. B* **93**, 235435 (2016).
- [33] P. Giannozzi, S. Baroni, N. Bonini, M. Calandra, R. Car, C. Cavazzoni, D. Ceresoli, G. L. Chiarotti, M. Cococcioni, I. Dabo, A. D. Corso, S. de Gironcoli, S. Fabris, G. Fratesi, R. Gebauer, U. Gerstmann, C. Gougoussis, A. Kokalj, M. Lazzeri, L. Martin-Samos, N. Marzari, F. Mauri, R. Mazzarello, S. Paolini, A. Pasquarello, L. Paulatto, C. Sbraccia, S. Scandolo, G. Sclauzero, A. P. Seitsonen, A. Smogunov, P. Umari, and R. M. Wentzcovitch, *J. Phys. Condens. Matter* **21**, 395502 (2009).
- [34] J. P. Perdew and A. Zunger, *Phys. Rev. B* **23**, 5048 (1981).
- [35] J. P. Perdew, M. Ernzerhof, and K. Burke, *J. Chem. Phys.* **105**, 9982 (1996).
- [36] J. Deslippe, G. Samsonidze, D. A. Strubbe, M. Jain, M. L. Cohen, and S. G. Louie, *Comput. Phys. Commun.* **183**, 1269 (2012).
- [37] G. Samsonidze, M. Jain, J. Deslippe, M. L. Cohen, and S. G. Louie, *Phys. Rev. Lett.* **107**, 186404 (2011).
- [38] S. Ismail-Beigi, *Phys. Rev. B* **73**, 233103 (2006).
- [39] J. Deslippe, G. Samsonidze, M. Jain, M. L. Cohen, and S. G. Louie, *Phys. Rev. B* **87**, 165124 (2013).
- [40] J. He, K. Hummer, and C. Franchini, *Phys. Rev. B* **89**, 075409 (2014).
- [41] K. S. Thygesen and A. Rubio, *Phys. Rev. Lett.* **102**, 046802 (2009).
- [42] J. B. Neaton, M. S. Hybertsen, and S. G. Louie, *Phys. Rev. Lett.* **97**, 216405 (2006).
- [43] M. Rohlfing, *Phys. Rev. Lett.* **108**, 087402 (2012).